Topological proximity effects in a Haldane graphene bilayer system

Peng Cheng,[1,*] Philipp W. Klein,[1,*] Kirill Plekhanov,[1,2,3] Klaus Sengstock,[4,5,6] Monika Aidelsburger,[7,8,9] Christof Weitenberg,[4,5] and Karyn Le Hur[1,†]

[1]*CPHT, CNRS, Ecole Polytechnique, Institut Polytechnique de Paris, Route de Saclay, F-91128 Palaiseau, France*
[2]*LPTMS, CNRS, Université Paris-Sud, Université Paris-Saclay, F-91405 Orsay, France*
[3]*Department of Physics, University of Basel, Klingelbergstrasse 82, CH-4056 Basel, Switzerland*
[4]*ILP–Institut für Laserphysik, Universität Hamburg, Luruper Chaussee 149, D-22761 Hamburg, Germany*
[5]*The Hamburg Centre for Ultrafast Imaging, Luruper Chaussee 149, D-22761 Hamburg, Germany*
[6]*Zentrum für Optische Quantentechnologien, Universität Hamburg, D-22761 Hamburg, Germany*
[7]*Fakultät für Physik, Ludwig-Maximilians-Universität, Schellingstrasse 4, D-80799 München, Germany*
[8]*Max-Planck-Institut für Quantenoptik, Hans-Kopfermann-Strasse 1, D-85748 Garching, Germany*
[9]*Munich Center for Quantum Science and Technology (MCQST), Schellingstrasse 4, D-80799 München, Germany*

We reveal a proximity effect between a topological band (Chern) insulator described by a Haldane model and spin-polarized Dirac particles of a graphene layer. Coupling weakly the two systems through a tunneling term in the bulk, the topological Chern insulator induces a gap and an opposite Chern number on the Dirac particles at half filling, resulting in a sign flip of the Berry curvature at one Dirac point. We study different aspects of the bulk-edge correspondence and present protocols to observe the evolution of the Berry curvature as well as two counterpropagating (protected) edge modes with different velocities. In the strong-coupling limit, the energy spectrum shows flat bands. Therefore we build a perturbation theory and address further the bulk-edge correspondence. We also show the occurrence of a topological insulating phase with Chern number one when only the lowest band is filled. We generalize the effect to Haldane bilayer systems with asymmetric Semenoff masses. Moreover, we propose an alternative definition of the topological invariant on the Bloch sphere.

Topological systems have attracted considerable attention these last decades [1,2] as they show robust gapless edge modes which are relevant for quantum information purposes [3]. The Haldane model [4] on the honeycomb lattice, which has been realized in ultracold atoms [5,6], graphene [7], quantum materials [8], and photonic topological systems [9–14], now appears as a paradigmatic model in the topological classification of Bloch energy bands. For spinless fermions, the bulk state is insulating at half filling and characterized by a topological invariant, the first Chern number, while the edges of the system reveal a one-dimensional gapless chiral mode by analogy with the quantum Hall effect [15–20]. Topological proximity effects induced by a topological band insulator [21–23] have also started to gain interest as a generalization of the proximity effect induced from a superconductor onto a metallic system [24,25]. Motivated by the recent interest in bilayer topological graphene systems [26], we study the proximity effect when tunnel coupling a Haldane model with a layer of graphene. Particle-hole processes at the interface open a gap as a result of pseudospin effects, inducing an inverse topological order in the graphene system when both layers are half filled.

We address different geometries to describe the bulk-edge correspondence and the Berry curvatures [27] of Bloch bands which could be equivalently probed for fermions and bosons at the one-particle level. We study the edge structure in relation with the Kane-Mele model [28–30] and with the quantum spin Hall effect at weak coupling [31,32]. We then address the strong-coupling flat-band limit and generalize the analysis to a bilayer Haldane model with asymmetric Semenoff masses [33]. We also suggest implementations in graphene bilayers, cold atoms, and photonic systems.

The Haldane model and graphene layers are described through the same pseudospin-1/2 representation in momentum space, as a result of the two sublattices of the honeycomb lattice [34], allowing us to describe the proximity effect in the same torus representation of the first Brillouin zone and fiber bundle approach on the Bloch sphere. In the latter case, we introduce an alternative description of the topological invariant.

The Hamiltonian takes the form $\mathcal{H} = \mathcal{H}_g + \mathcal{H}_h + \mathcal{H}_r$, where $\mathcal{H}_g$ describes the graphene layer [35–37], $\mathcal{H}_h$ the topological Haldane model, and $\mathcal{H}_r$ the tunnel coupling between the layers with amplitude r. For simplicity, below we present the results for a tunnel coupling r involving the same sublattice in the two layers. In the Supplemental Material, we show that this proximity effect is robust towards a more general choice of coupling parameters between the two subsystems [38]. We introduce the standard definitions where t_1 means the nearest-neighbor hopping element on the honeycomb lattice, and t_2 the second-nearest-neighbor tunneling element with the associated Peierls phases $\pm\Phi$ for sublattices A and B

---

*These authors contributed equally to this work.
†karyn.le-hur@polytechnique.edu

[38]. In wave-vector space, the Hamiltonian takes the form $\mathcal{H} = \int d\mathbf{k}/(2\pi^2)\mathcal{H}(\mathbf{k})$, where

$$\mathcal{H}(\mathbf{k}) = \begin{pmatrix} \mathbf{d}^g \cdot \boldsymbol{\sigma} & r \cdot \mathcal{I} \\ r \cdot \mathcal{I} & \mathbf{d}^h \cdot \boldsymbol{\sigma} + \epsilon_h \cdot \mathcal{I} \end{pmatrix}, \qquad (1)$$

with the vector σ of Pauli matrices acting in the Hilbert space of sublattice A and sublattice B of each layer g and h, respectively [34]. Particles are assumed to be spin-less (spin polarized). To make an analogy with two $1/2$ spins in $\mathbf{k}$ space, one could also choose to introduce two different sets of Pauli matrices $\boldsymbol{\sigma}^g$ and $\boldsymbol{\sigma}^h$ acting in the sublattice space of each layer; the results derived below can be simplified in notations through the introduction of one set of Pauli matrices. The magnetic fields are $d_x^h(\mathbf{k}) = -t_1 \sum_{i=1}^3 \cos(\mathbf{k} \cdot \mathbf{a}_i)$, $d_y^h(\mathbf{k}) = -t_1 \sum_{i=1}^3 \sin(\mathbf{k} \cdot \mathbf{a}_i)$, and $d_z^h(\mathbf{k}) = -2t_2 \sin \Phi \sum_{i=1}^3 \sin(\mathbf{k} \cdot \mathbf{b}_i)$. The vectors $\mathbf{a}_i$ and $\mathbf{b}_i$ link nearest neighbors and next-nearest neighbors on the honeycomb lattice [38]. Furthermore, $\epsilon_h = -2t_2 \cos \Phi \sum_{i=1}^3 \cos(\mathbf{k} \cdot \mathbf{b}_i)$ and $\mathcal{I}$ is the 2×2 identity matrix acting in the sublattice space of the different layers. Since we assume that the nearest-neighbor tunneling amplitudes are identical in both layers (for the simplicity of notations but without loss of generality), then $d_x^g(\mathbf{k}) = d_x^h(\mathbf{k})$ and $d_y^g(\mathbf{k}) = d_y^h(\mathbf{k})$, and initially for graphene (when $r = 0$) the magnetic field in $\mathbf{k}$ space resides in the equatorial plane $d_z^g(\mathbf{k}) = 0$. In the numerical calculations below, we fix the phase $\Phi = \pi/2$.

Mapping the first Brillouin zone on a torus onto the sphere S^2, the Haldane model at $r = 0$ is characterized by the normalized magnetic field $d^* = [\sin \theta(\mathbf{k}) \cos \phi(\mathbf{k}), \sin \theta(\mathbf{k}) \sin \phi(\mathbf{k}), \cos \theta(\mathbf{k})]$ such that the Chern number associated with the two bands of the topological Haldane insulator can be defined as

$$C_\pm^h = \frac{1}{2\pi} \int_{S^2} F_\pm = \mp \frac{1}{4\pi} \int_{S^2} d\Omega = \mp 1, \qquad (2)$$

with the relation between the Berry curvature and the solid angle on the sphere S^2, $F_\pm = \mp \sin \theta d\theta d\phi = \mp \frac{d\Omega}{2}$. In Fig. 1 (top left), we show the Berry curvature associated with the lowest-energy band of the Haldane model, corresponding to the Chern number $C_-^h = C_1 = +1$. The Chern number of such spin-$1/2$ models on the sphere S^2 has been measured in circuit quantum electrodynamics [39–41]. The Berry curvature of the Haldane model has also been measured in cold atoms [6] through the momentum distribution [6,42]. The topology of Bloch bands can also be accessed through Wilson line measurements [43] and coupling with circularly polarized
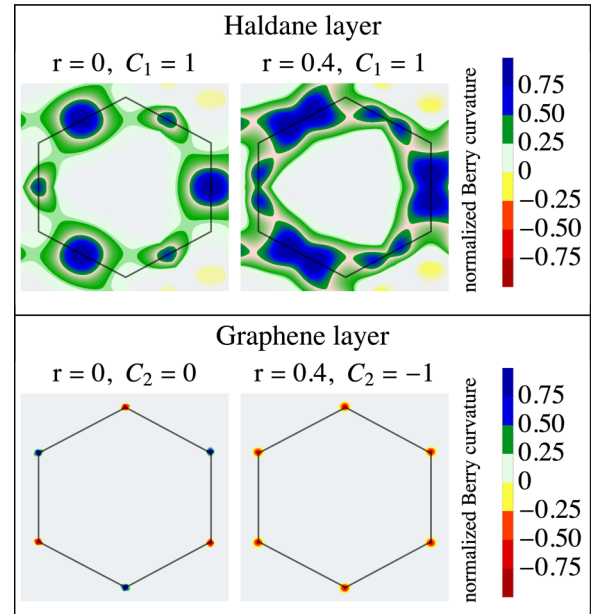

FIG. 1. Berry curvature in the Brillouin zone for the Haldane and graphene layers at $r = 0$ and small r, showing the Berry phase jump effect [38]. Here, $t_1 = 1$ and $t_2 = 1/3$. Results in the Haldane layer remain almost unchanged from $r = 0$ to $r = 0.4$: The pseudospin $1/2$ is polarized close to the Dirac point, and the dominant contribution to the Berry curvature occurs close to the highly symmetric M points [38].

light [7,44]. The Chern number of graphene is equal to $C_\pm^g = C_2 = 0$ when $r = 0$. One can still define a Berry phase [27] $\pm \pi$ associated with pseudospin effects around the two inequivalent Dirac points $\pm \mathbf{K}$ ($\mathbf{K}$ and $\mathbf{K}'$) (see Fig. 1) [35].

To show how an effective d_z^g magnetic field component can be induced in the graphene layer through the presence of the d_z^h term in the Haldane system, we build a perturbation theory and a path integral approach in the small $r \ll (t_1, t_2)$ limit by integrating out degrees of freedom of the Haldane model and revealing particle-hole processes at the interface; see Supplemental Material [38]. A particle starts from, say, graphene in sublattice A (B), then takes the same sublattice in the Haldane layer, and after the action of the second-nearest-neighbor tunneling term t_2 giving a phase $+\Phi$ ($-\Phi$), the particle goes back in the graphene lattice, producing an effective d_z^g term with $t_2^{\text{eff}} \sim -|r|^2/(27t_2^2 \sin^2 \Phi)t_2$; the minus sign is a result of second-order perturbation theory [22]. The partition function of the graphene layer becomes [38]

$$Z_g = \int \mathcal{D}\zeta_g(\mathbf{k}) \mathcal{D}\bar{\zeta}_g(\mathbf{k}) \exp -\left(\int_0^\beta d\tau \int \frac{d^2k}{2\pi^2} \bar{\zeta}_g(\mathbf{k}) \left[\partial_\tau + \mathbf{d}^g(\mathbf{k})\sigma - \frac{|r|^2}{||\mathbf{d}^h(\mathbf{k})||^2}(1 - e^{-\epsilon\tau})\mathbf{d}^h(\mathbf{k})\sigma \right] [\zeta_g(\mathbf{k})]^T \right), \qquad (3)$$

with $\zeta_g(\mathbf{k}) = [c_{gA}(\mathbf{k}), c_{gB}(\mathbf{k})]$ describing a fermion operator in the graphene layer, at sublattice A and B, respectively, and ϵ an energy scale close to t_2. At long timescales $\epsilon\tau \gg 1$ or low energy compared to the Haldane gap we find that the proximity effect indeed results in the induction of a magnetic field in the graphene layer along the z direction. In

the Supplemental Material [38], we build an analogy with an Ising coupling between two spins-$1/2$ impurities $\boldsymbol{\sigma}^g$ and $\boldsymbol{\sigma}^h$ in reciprocal space.

Then, we derive an effective low-energy model close to the Dirac points of graphene ($d_x = d_y \sim 0$), approximating $d_z^h(\mathbf{k} \sim \pm \mathbf{K}) = \pm 3\sqrt{3}t_2 \sin \Phi$. By analogy

to the Haldane model, the induced mass term is $\sim -|r|^2/(27t_2^2 \sin^2 \Phi)d_z^h(\mathbf{k})\sigma_z$. This now ensures that the low-energy band of the graphene layer satisfies the following condition on the Chern number $C_-^g = C_2 = -1$.

To understand this key point, we use the form of the eigenstates close to a given Dirac point in graphene [35],

$$\frac{1}{\sqrt{2}}\begin{pmatrix} 1 \\ \pm e^{i\phi(\mathbf{q})} \end{pmatrix}, \tag{4}$$

where $\mathbf{q}$ corresponds to a small deviation from a Dirac point such that $\tan\phi = q_y/q_x$. The $\pm$ signs refer to positive energy and negative energy bands respectively meeting at the Dirac point; these two bands are related through $\phi \leftrightarrow \phi + \pi$. It is constructive to introduce the induced mass (gap) $m = -|r|^2/(27 \sin^2 \Phi t_2^2)d_z^h(\mathbf{k})$, which changes of sign at the two Dirac points in the graphene layer. In the Supplemental Material, we provide the forms of the eigenstates as a function of $v_F||\mathbf{q}||$ and m [38]. We check that eigenstates converge to those of Eq. (4) in the limit $|m| \ll v_F||\mathbf{q}||$, where $v_F = 3t_1 a/2$ is the Fermi velocity and a the lattice spacing. The two Dirac points $\mathbf{K}$ and $\mathbf{K}'$ are now related through a mass $m \to -m$ inversion corresponding to change $\phi \to \phi' = -\phi + \pi$. The operation $\phi \to -\phi$ corresponds to the change $\mathbf{K}$ in $\mathbf{K}'$ and the additional π phase corresponds to inverting the upper and lower bands. We find that the Berry phases around the two Dirac points become equal [38],

$$\gamma_K = \gamma_{K'} = -\frac{1}{2}\oint \nabla\phi(\mathbf{k}) \cdot d\mathbf{k} = -\pi. \tag{5}$$

The integration follows a closed path around a Dirac point. We numerically check [45] that a $-\pi$ Berry phase occurs at both Dirac points of graphene (see Fig. 1), similarly to the Haldane model when $t_2 \ll t_1$. We also check that for the upper band of graphene, $C_+^g = +1 = -C_+^h$ or $\gamma_K = \gamma_{K'} = \pi$ (this is equivalent to changing $m \to -m$ at a Dirac point or $d_z^h \to -d_z^h$; see also the Supplemental Material in Ref. [38]). Progress on engineering twisted bilayer graphene systems has recently allowed one to achieve new band structures, and Dirac fermions with opposite chiralities have recently been observed [46]. Then, by applying circularly polarized light [7], one could already achieve two topological bands showing opposite Chern numbers. Below, we shall engineer a specific bilayer graphene model which can be realized in cold atoms.

The Berry phases could be directly measured as demonstrated in Refs. [6,43,47]. Information on Berry phases could also be reconstructed from quantum Hall conductivity [19,48] quantum circular dichroism by shining light [44], scanning probe [49,50], and Klein paradox [51,52] measurements.

Now, we study in more detail the edge properties. For two layers of equal size, for $r \neq 0$, we find the formation of a gap at the edges at half filling, resulting from the hybridization of the zigzag edge mode of graphene—present at $r = 0$—with the topological edge mode [see the black edge modes in Fig. 2 (left) corresponding to the right boundary of the green cylinder]. This is also consistent with the Kane-Mele model [53], where the r coupling at the edges corresponds to a spin-flip process which breaks the $\mathcal{Z}_2$ symmetry and opens a gap similar to the effect of the Mott transition [54,55]. To confirm that a chiral edge state has now appeared in the graphene layer at half filling moving in the opposite direction as the edge state
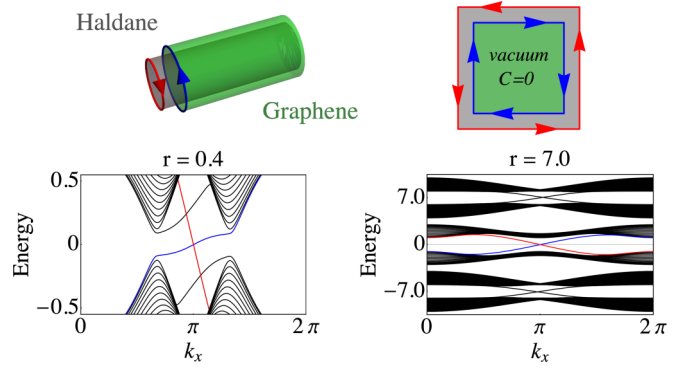

FIG. 2. Cylinder representations of the Haldane (in gray) and graphene (in green) systems, in the wave-vector space. The green region has 60 unit cells and the gray region has 14 additional unit cells. Band structures for $t_1 = 1$ and $t_2 = 1/3$ in the weak- and strong-coupling limits for this cylinder geometry [1]; the lattice spacing is $a = 1$. On the left, we zoom on the two low-energy graphene bulk bands. We observe two counterpropagating edge modes with different velocities at zero energy for r of the order of t_2. For very strong couplings, on the right, the counterpropagating edge modes at low energy are only linked to the Haldane region, and the central strongly hybridized region becomes identical to the vacuum (or becomes topologically trivial).

in the Haldane layer, in agreement with $(C_-^h - C_-^g) = 2$ in the bulk for $r \neq 0$ [56], we suggest to suppress smoothly the r tunnel coupling at the left edge. In the numerics, we check that for more additional 10 unit cells in the Haldane region, the results are stable: Fig. 2 then shows two counterpropagating edge modes with different velocities, due to the different gaps in the two layers, crossing the chemical potential at half filling (or energy zero). Alternatively, one could build a slightly smaller layer and observe two counterpropagating edge modes, one in each layer (see Fig. 2, top right).

To address the strong-coupling limit $r \gg (t_1, t_2)$ analytically, we define the field operators $\psi_\pm = 1/\sqrt{2}(c_{gA} \pm c_{hA})$ hybridizing the sublattices A of the two layers and $\chi_\pm = 1/\sqrt{2}(c_{gB} \pm c_{hB})$ hybridizing the sublattices B of the two layers. Similarly to the graphene layer in Eq. (3), $c_{hA}^\dagger$ and $c_{hB}^\dagger$ represent creation operators at sublattices A and B in the Haldane layer. To show that the strong-coupling description is very general we introduce the magnetic fields $\mathbf{d}_1$ and $\mathbf{d}_2$ associated with the two layers, that we shall rewrite in the hybridized basis. To find the effective Hamiltonian in the basis $[\psi_-, \chi_-, \psi_+, \chi_+]$, we can equivalently perform a unitary transformation, such that the Hamiltonian becomes

$$\tilde{\mathcal{H}}(\mathbf{k}) = \begin{pmatrix} -r\mathcal{I} + \frac{(\mathbf{d}_1+\mathbf{d}_2)}{2} \cdot \boldsymbol{\sigma} & \frac{(\mathbf{d}_1-\mathbf{d}_2)}{2} \cdot \boldsymbol{\sigma} \\ \frac{(\mathbf{d}_1-\mathbf{d}_2)}{2} \cdot \boldsymbol{\sigma} & r\mathcal{I} + \frac{(\mathbf{d}_1+\mathbf{d}_2)}{2} \cdot \boldsymbol{\sigma} \end{pmatrix}. \tag{6}$$

The energy spectrum shows two pairs of bands centered around $\pm r$ (see Ref. [38]) and described by a Haldane model with an effective magnetic field in $\mathbf{k}$ space which gives rise to $(\mathbf{d}_1 + \mathbf{d}_2) \cdot \boldsymbol{\sigma}/2$. The off-diagonal terms couple band pairs of different energy which do not affect the low-energy theory. For the Haldane graphene bilayer with $\mathbf{d}_1 = \mathbf{d}^g$ and $\mathbf{d}_2 = \mathbf{d}^h$, Berry curvatures of the two lowest bands for $r \gg t_2$ are shown in Fig. 3.
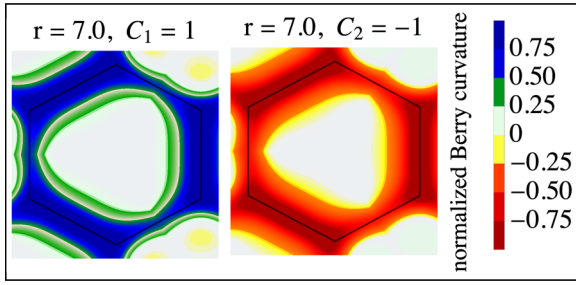
FIG. 3. Berry curvatures for the two lowest-energy bands at strong coupling $r = 7$ ($t_1 = 1$ and $t_2 = 1/3$).

In Fig. 2, the two lowest "hybrid" bands are still described by a total Chern number zero and the bulk green region now behaves as the vacuum, i.e., it becomes topologically trivial. In Fig. 2, we now observe two counterpropagating edge modes with equal velocities at zero energy, when suppressing the tunnel coupling at one edge in the cylinder geometry (in the gray region). By making one layer slightly larger than the other, the two edge modes now entirely connect to the Haldane bulk bands of the gray region.

At quarter filling [implying that the particle densities of the two layers satisfy ($n_g = n_h = 1/4$)] only the lowest band in Fig. 2 (right) should be filled, and the system reveals a topological phase with Chern number 1. The edge structure shows on average 1/2 particle in one layer moving together with 1/2 particle in the other layer.

We now address the situation of a Haldane model in each layer with $\mathbf{d}_1 = \mathbf{d}_2 = \mathbf{d}^h$ which can be realized in ultracold atoms through a shaking protocol, resulting in $t_2 \ll t_1$ [38]. We predict an evolution from a phase with total Chern number $C = 2$ to a phase with total Chern number 0, when increasing r [38]. This demonstrates that the topological proximity effect subsists in the case of two coupled insulators [23]. We now discuss the effect of Semenoff masses M_1 and M_2 in the two layers [33]. This results in an additional term $(M_1 + M_2)\sigma_z/2$ in Eq. (6) in the subspace $[\psi_-, \chi_-]$ and similarly for the subspace $[\psi_+, \chi_+]$. For asymmetric masses, we find two transitions showing a jump of the Berry phase at one Dirac point only (as discussed above for a graphene layer weakly coupled to a Haldane Chern insulator), namely, the $\mathbf{K}'$ and then the $\mathbf{K}$ point, and the bands remain distinguishable in the intermediate $C = 1$ region (see Fig. 4). We present the gap evolution and additional information in the Supplemental Material for this situation, that may be realized in ultracold atoms [38]. For $M_1 = M_2$, a band touching effect occurs, then suppressing the $C = 1$ region [38].

Below, we present an alternative description of the topological proximity effect on the Bloch sphere with polar angle $\theta(\mathbf{k})$ and azimuthal angle $\phi(\mathbf{k})$, defining the Haldane model at $r = 0$. From Stokes' theorem, for $r \neq 0$, we rewrite the Chern number of the different bands in the equatorial plane for an angle $\theta(\mathbf{k}) = \pi/2$ as

$$C_j = \frac{1}{2\pi} \int_0^{2\pi} d\phi \left(\langle \psi_N^j | i\frac{\partial}{\partial \phi} | \psi_N^j \rangle - \langle \psi_S^j | i\frac{\partial}{\partial \phi} | \psi_S^j \rangle \right), \quad (7)$$

where $|\psi_N^j\rangle = |\psi_j(\theta(\mathbf{k}), \phi(\mathbf{k}), N)\rangle$ and $|\psi_S^j\rangle = |\psi_j(\theta(\mathbf{k}), \phi(\mathbf{k}), S)\rangle$ are eigenstates corresponding to the band j defined
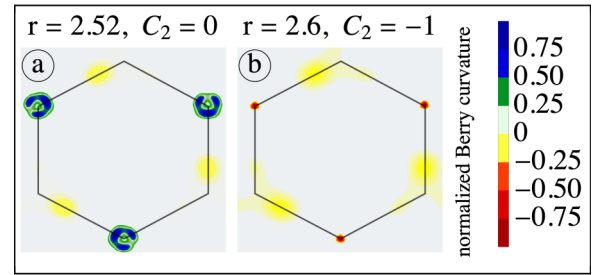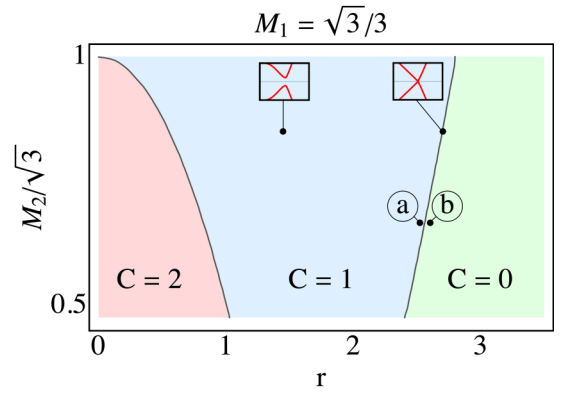

FIG. 4. Numerical phase diagram for two coupled Haldane models with $\mathbf{d}_1 = \mathbf{d}_2 = \mathbf{d}^h$. Evolution of the total Chern number C for the two lowest bands as a function of r and M_2 for $M_1 = 1/\sqrt{3}$ in units of $t_1 = 1$ and $t_2 = 1/3$. Illustration of Berry phase "jumps" at the second phase transition.

in the north (N) or south (S) hemisphere [38]. Going from the north to south pole is equivalent to modifying the vectors $\mathbf{a}_i \rightarrow -\mathbf{a}_i$ and $\mathbf{b}_i \rightarrow -\mathbf{b}_i$ in real space (if we fix $\mathbf{k}$). This is also equivalent to changing the role of sublattices A and B in each layer. We check that for the lowest-energy band corresponding to the valence band of the Haldane model in weak coupling, then $C_1 = C_-^h = +1$. The two lowest bands (and also the two upper energy bands) acquire opposite winding phases due to the relative phase fixing the argument at the north pole when $r \neq 0$, i.e., $C_2 = C_-^g = -1$, encoding the mass inversion effects between bands. We justify the equivalence between Eqs. (2) and (7) in Ref. [38].

To summarize, we have presented a proximity effect from a topological Chern insulator on a graphene layer. The two lowest filled energy bands show inverse Chern numbers $+1$ and -1. We have illustrated the bulk-edge correspondence in relation with the Kane-Mele model [28,56], and with general bulk-edge correspondence in the ultrastrong-coupling limit. Progress on twisted bilayer systems [46] and coupling with circularly polarized light [7] could allow one to engineer such a topological proximity effect. In the Supplemental Material, we discuss implementations in cold-atom bilayers in relation to Fig. 4 and light systems thoroughly. Interaction effects leading to a Mott transition [54,55,57,58] and fractional quantum Hall phases will be studied further [59].

[1] B. A. Bernevig and T. L. Hughes, *Topological Insulators and Topological Superconductors* (Princeton University Press, Princeton, NJ, 2013).

[2] M. Z. Hasan and C. L. Kane, Rev. Mod. Phys. **82**, 3045 (2010); J. E. Moore, Nature (London) **464**, 194 (2010).

[3] C. Nayak, S. H. Simon, A. Stern, M. Freedman, and S. Das Sarma, Rev. Mod. Phys. **80**, 1083 (2008).

[4] F. D. M. Haldane, Phys. Rev. Lett. **61**, 2015 (1988).

[5] G. Jotzu, M. Messer, R. Desbuquois, M. Lebrat, T. Uehlinger, D. Greif, and T. Esslinger, Nature (London) **515**, 237 (2014).

[6] N. Fläschner, B. S. Rem, M. Tarnowski, D. Vogel, D.-S. Lühmann, K. Sengstock, and C. Weitenberg, Science **352**, 1091 (2016).

[7] J. W. McIver, B. Schulte, F.-U. Stein, T. Matsuyama, G. Jotzu, G. Meier, and A. Cavalleri, arXiv:1811.03522.

[8] C.-X. Liu, S.-C. Zhang, and X.-L. Qi, Annu. Rev. Condens. Matter Phys. **7**, 301 (2016).

[9] F. D. M. Haldane and S. Raghu, Phys. Rev. Lett. **100**, 013904 (2008).

[10] L. Lu, J. D. Joannopoulos, and M. Soljacic, Nat. Photonics **8**, 821 (2014).

[11] M. C. Rechtsman, J. M. Zeuner, Y. Plotnik, Y. Lumer, D. Podolsky, F. Dreisow, S. Nolte, M. Segev, and A. Szameit, Nature (London) **496**, 196 (2013).

[12] J. Koch, A. A. Houck, K. Le Hur, and S. M. Girvin, Phys. Rev. A **82**, 043811 (2010).

[13] K. Le Hur, L. Henriet, A. Petrescu, K. Plekhanov, G. Roux, and M. Schiró, C. R. Phys. **17**, 808 (2016).

[14] T. Ozawa, H. M. Price, A. Amo, N. Goldman, M. Hafezi, L. Lu, M. C. Rechtsman, D. Schuster, J. Simon, O. Zilberberg, and I. Carusotto, Rev. Mod. Phys. **91**, 015006 (2019).

[15] K. V. Klitzing, G. Dorda, and M. Pepper, Phys. Rev. Lett. **45**, 494 (1980).

[16] K. S. Novoselov, Z. Jiang, Y. Zhang, S. V. Morozov, H. L. Stormer, U. Zeitler, J. C. Maan, G. S. Boebinger, P. Kim, and A. K. Geim, Science **315**, 1379 (2007).

[17] B. I. Halperin, Phys. Rev. B **25**, 2185 (1982).

[18] M. Büttiker, Phys. Rev. B **38**, 9375 (1988).

[19] D. J. Thouless, M. Kohmoto, M. P. Nightingale, and M. den Nijs, Phys. Rev. Lett. **49**, 405 (1982).

[20] M. Kohmoto, Ann. Phys. **160**, 343 (1985).

[21] T. Shoman, A. Takayama, T. Sato, S. Souma, T. Takahashi, T. Oguchi, K. Segawa, and Y. Ando, Nat. Commun. **6**, 6547 (2015).

[22] T. H. Hsieh, H. Ishizuka, L. Balents, and T. L. Hughes, Phys. Rev. Lett. **116**, 086802 (2016).

[23] J.-H. Zheng and W. Hofstetter, Phys. Rev. B **97**, 195434 (2018).

[24] K. Le Hur, Phys. Rev. B **64**, 060502(R) (2001); K. Le Hur and T. M. Rice, Ann. Phys. **324**, 1452 (2009).

[25] K. Le Hur, S. Vishveshwara, and C. Bena, Phys. Rev B **77**, 041406(R) (2008).

[26] J. D. Sanchez-Yamagishi, J.-Y. Luo, A.-F. Young, B. Hunt, K. Watanabe, T. Taniguchi, R. C. Ashoori, and P. Jarillo-Herrero, Nat. Nanotechnol. **12**, 118 (2017).

[27] M. V. Berry, Proc. R. Soc. London, Ser. A **392**, 45 (1984).

[28] C. L. Kane and E. J. Mele, Phys. Rev. Lett. **95**, 226801 (2005).

[29] B. A. Bernevig and S. C. Zhang, Phys. Rev. Lett. **96**, 106802 (2006).

[30] S. Murakami, Phys. Rev. Lett. **97**, 236805 (2006).

[31] M. König, S. Wiedmann, M. Brüne, A. Roth, H. Buhmann, L. W. Molenkamp, X.-L. Qi, and S.-C. Zhang, Science **318**, 766 (2007).

[32] S. Wu, V. Fatemi, Q. D. Gibson, K. Watanabe, T. Taniguchi, R. J. Cava, and P. Jarillo-Herrero, Science **359**, 76 (2018).

[33] G. W. Semenoff, Phys. Rev. Lett. **53**, 2449 (1984).

[34] J. Cayssol, C. R. Phys. **14**, 760 (2013).

[35] A. H. Castro Neto, F. Guinea, N. M. R. Peres, K. S. Novoselov, and A. K. Geim, Rev. Mod. Phys. **81**, 109 (2009).

[36] P. Soltan-Panahi, D.-S. Lühmann, J. Struck, P. Windpassinger, and K. Sengstock, Nat. Phys. **8**, 71 (2012).

[37] L. Tarruell, D. Greif, T. Uehlinger, G. Jotzu, and T. Esslinger, Nature (London) **483**, 302 (2012).

[38] See Supplemental Material at http://link.aps.org/supplemental/10.1103/PhysRevB.100.081107 for additional information on: definitions of the two systems and coupling parameters, topological proximity effect and notations related to numerical evaluations of Berry curvatures; mathematical arguments related to the Berry phase shift and the alternative derivation of the topological invariant on the Bloch sphere; implementations and protocols in cold atoms and photonic systems, for the Haldane bilayer model with two Semenoff masses.

[39] P. Roushan, C. Neill, Y. Chen, M. Kolodrubetz, C. Quintana, N. Leung, M. Fang, R. Barends, B. Campbell, Z. Chen *et al.*, Nature (London) **515**, 241 (2014).

[40] M. D. Schroer, M. H. Kolodrubetz, W. F. Kindel, M. Sandberg, J. Gao, M. R. Vissers, D. P. Pappas, A. Polkovnikov, and K. W. Lehnert, Phys. Rev. Lett. **113**, 050402 (2014).

[41] L. Henriet, A. Sclocchi, P. P. Orth, and K. Le Hur, Phys. Rev. B **95**, 054307 (2017); K. Le Hur, L. Henriet, L. Herviou, K. Plekhanov, A. Petrescu, T. Goren, M. Schiro, C. Mora, and P. P. Orth, C. R. Phys. **19**, 451 (2018).

[42] P. Hauke, M. Lewenstein, and A. Eckardt, Phys. Rev. Lett. **113**, 045303 (2014).

[43] T. Li, L. Duca, M. Reitter, F. Grusdt, E. Demler, M. Endres, M. Schleier-Smith, I. Bloch, and U. Schneider, Science **352**, 1094 (2016).

[44] L. Asteria, D. T. Tran, T. Ozawa, M. Tarnowski, B. S. Rem, N. Fläschner, K. Sengstock, N. Goldman, and C. Weitenberg, Nat. Phys. **15**, 449 (2019).

[45] T. Fukui, Y. Hatsugai, and H. Suzuki, J. Phys. Soc. Jpn. **74**, 1674 (2005).

[46] K. S. Kim, A. L. Walter, L. Moreschini, T. Seyller, K. Horn, E. Rotenberg, and A. Bostwick, Nat. Mater. **12**, 887 (2013).

[47] L. Duca, T. Li, M. Reitter, I. Bloch, M. Schleier-Smith, and U. Schneider, Science **347**, 288 (2015).

[48] M. Aidelsburger, M. Lohse, C. Schweizer, M. Atala, J. T. Barreiro, S. Nascimbène, N. R. Cooper, I. Bloch, and N. Goldman, Nat. Phys. **11**, 162 (2015).

[49] M. Braun, L. Chirolli, and G. Burkard, Phys. Rev. B **77**, 115433 (2008).

[50] M. A. Topinka, R. M. Westervelt, and E. J. Heller, Phys. Today **56** (12), 47 (2003).

[51] M. I. Katsnelson, K. S. Novoselov, and A. K. Geim, Nat. Phys. **2**, 620 (2006).

[52] N. Stander, B. Huard, and D. Goldhaber-Gordon, Phys. Rev. Lett. **102**, 026807 (2009).

[53] L. Fu and C. L. Kane, Phys. Rev. B **76**, 045302 (2007).

[54] W. Wu, S. Rachel, W.-M. Liu, and K. Le Hur, Phys. Rev. B **85**, 205102 (2012).

[55] S. Rachel and K. Le Hur, Phys. Rev. B **82**, 075106 (2010).

[56] D. N. Sheng, Z. Y. Weng, L. Sheng, and F. D. M. Haldane, Phys. Rev. Lett. **97**, 036808 (2006).

[57] I. Vasić, A. Petrescu, K. Le Hur, and W. Hofstetter, Phys. Rev. B **91**, 094502 (2015).

[58] K. Plekhanov, I. Vasić, A. Petrescu, R. Nirwan, G. Roux, W. Hofstetter, and K. Le Hur, Phys. Rev. Lett. **120**, 157201 (2018).

[59] S. Sorn, Phys. Rev. B **98**, 125145 (2018).